Global and Seasonal Variations in Three-Dimensional Gravity Wave Momentum Flux from Satellite Limb Sounding Temperatures

M. J. Alexander,[1]

Corresponding author: M. J. Alexander, NorthWest Research Associates, 3380 Mitchell Lane, Boulder, CO 80301, USA. (alexand@nwra.com)

[1]NorthWest Research Associates,

Boulder, Colorado, USA.

Satellite limb sounding methods provide the best global temperature data available for simultaneous measurement of gravity wave horizontal and vertical structure needed to estimate momentum flux and constrain wave effects on general circulation. Gravity waves vary in the three spatial dimensions and time, so the ideal measurement observes all three dimensions at high resolution nearly simultaneously. High Resolution Dynamics Limb Sounder (HIRDLS) measurements, give near-simultaneous profiles in close proximity and at high vertical resolution, but these coincident profiles lie only along the plane of the measurement track. Here we combine HIRDLS and radio occultation datasets to obtain three-dimensional properties of gravity waves on a global scale as well as seasonal variations. The results show dramatic changes from previous estimates using either dataset alone. Changes include much larger momentum fluxes and latitudinal variations in propagation direction that support an enhanced role for gravity wave forcing of middle atmosphere circulation.

1. Introduction

The effects of small-scale gravity waves on the circulation of the upper troposphere and middle atmosphere are well appreciated, and hence these unresolved waves are included via parameterization in global models that are used for climate projections, weather forecasting, and data assimilation. (See *Alexander et al.* [2010] for a review.) The so called "gravity wave drag" has a leading order effect on circulation in the mesosphere and substantially reduces wind and temperature biases near the tropopause and in the stratosphere where gravity waves can influence planetary wave propagation, teleconnection pathways, polar temperatures, and ozone chemistry. It remains a challenge to observe properties of small-scale gravity waves to constrain gravity wave drag parameterizations on a global scale [*Geller et al.*, 2013].

In Geller et al. [2013] gravity wave momentum fluxes derived from limb sounding temperature measurements was compared to gravity waves resolved in two high-resolution models and parameterized gravity waves in three climate models. Temperature profiles from HIRDLS have the best combined global coverage and resolution of any of the observational estimates included in the Geller et al. [2013] comparison. The global and seasonally varying patterns in the observations strongly resembled the patterns seen in gravity waves resolved in high-resolution models. The parameterized fluxes failed to show some of these patterns, and so the observations provided useful constraints in that sense.

On the other hand, momentum fluxes from high-inclination limb-sounding measurements like HIRDLS are known to be biased low, but to an unknown degree [*Alexander et al.*, 2008; *Ern et al.*, 2011]. The comparison to the models in *Geller et al.* [2013] suggested HIRDLS may be biased low by a factor of about 2–4 in the lower stratosphere near 20 km, although this remains a coarse estimate due to the uncertainties in all the methods compared. A key conclusion of that study was that the parameterized gravity waves in the climate models were all very similar despite the fact that the three models used three different orographic gravity wave parameterizations, and three different non-orographic gravity wave parameterizations. The global-mean parameterized momentum fluxes in the three climate models only differed from each other by $\pm 12\%$, which stands in stark contrast to the likely factor of 2–4 uncertainty in the magnitudes of the global observations. The inference is that the climate model simulations are all similar because they have tuned their parameterizations to get a realistic circulation. Therefore, regarding total momentum flux, the climate models are constraining themselves better than the observations are able to at the present time. The climate models still struggle to obtain realistic circulation patterns near the tropopause and in the mesosphere simultaneously, and despite decades of research, south polar stratospheric temperatures tend to be excessively cold and winds excessively strong in many state of the art models [*Butchart et al.*, 2011]. Recent research has also shown that the details of the parameterization methods can dramatically effect predictions of future circulation changes [*Schirber et al.*, 2015]. Hence progress in more accurate observations of gravity wave momentum fluxes are needed.

The problem plaguing the orbiting limb-sounding observations like HIRDLS is the essentially two-dimensional (2D) nature of the analysis. The data include high-vertical resolution temperature profiles, but the horizontal spacing is limited, and most importantly, the horizontal wavenumber that is estimated is determined only along the measurement track.

Figure 1a shows how sampling only along this 2D plane limits the wavenumber measured to an "apparent horizontal wavenumber", whereas the true wavenumber will generally lie at some other angle. Hence the horizontal wavelength is generally over-estimated, and sometimes to an extreme degree. Section 2 explains how this over-estimation results in a proportional under-estimation of the momentum flux.

Temperature profiles from Global Positioning System radio occultation (GPSRO), particularly from the Constellation Observing System for Meteorology (COSMIC) mission [*Anthes et al.*, 2008] do not have this same limitation, but instead obtain profiles at rather random positions globally. However, the measurements are only rarely closely spaced in both space and time. To use adjacent profiles to infer horizontal wavenumber requires the assumption that the wave phase is unchanged during the time interval between adjacent profiles. For HIRDLS, this time spacing Δt is only seconds, much shorter than gravity wave periods, and hence the assumption is excellent. For COSMIC GPSRO, restricting adjacent profiles to similar times leads to very few close coincidences. *Wang and Alexander* [2010] attempted a statistical approach to inferring wave properties from neighboring profiles collected over 4 hrs because the GPSRO sampling was inadequate for determination of global variations in gravity wave momentum flux. More recently, *Faber et al.* [2013] derived momentum fluxes from GPSRO profile triads obtained within 2 hrs and 10°, but even this sampling restriction is insufficient for accurate momentum flux determination.

Here, combined measurements from HIRDLS and COSMIC are used to obtain global and seasonal variations in momentum flux. *Wright et al.* [2011] showed that the effective vertical resolution of gravity wave temperature anomalies was very similar for HIRDLS and GPSRO data, both resolving features ∼1 km. Although the combined data coverage remains limited, biases in the derived momentum flux are greatly reduced. The focus here will be on results in the lower stratosphere, where the values can represent the input momentum fluxes to the middle atmosphere and the results may be most valuable for climate modeling.

2. Data and Methodology

2.1. HIRDLS temperature measurements and 2D momentum flux estimates

The High-Resolution Dynamics Limb Sounder (HIRDLS) provided temperature profiles at altitudes above cloud top to an altitude of 80 km in the mesosphere. Vertical scans were completed every 8s giving nominal spacings between adjacent profiles of ∼ 100 km. The dimensions of the detector slit projected on Earth's limb was 10 km × 1.2 km in the horizonal and vertical, respectively [Gille et al., 2008]. Typically, over 5500 profiles were obtained each day and provided on a 750m vertical grid in log-pressure altitude. The temperature precision is reported at less than 0.5K between 20-50 km [*Gille and et al.*, 2008]. Temperature retrievals below 60 km have not changed since Version 5. We use the Version 6 temperatures here, and to match GPSRO coverage, we use temperatures only below 40 km. HIRDLS measurements begin in January 2005 and extend until March 2008. HIRDLS gravity wave temperature anomalies are derived after removal of a background temperature as described in supporting information S1.

2.2. Two-dimensional gravity wave analysis

Temperature profiles observed with HIRDLS have been used to estimate global patterns in gravity wave momentum flux in many studies [*Alexander et al.*, 2008; *Wright et al.*, 2010; *France et al.*, 2012; *Ern et al.*, 2011]. These methods use temperature profiles to estimate the vertical wavelength λ_Z spectrum and covarying signals in adjacent profiles are used to estimate the horizontal wavelength measured along the line joining the two profiles [Ern et al., 2004]. We call this wavelength the "apparent wavelength" λ_A to distinguish it from the true horizontal wavelength λ_T that would be measured if at least three profiles forming a triangle were instead available. (See Figure 1.) The momentum flux M_{2D} estimated using these two-dimensional methods is given by

$$M_{2D} = \frac{\bar{\rho}}{2}\frac{\lambda_Z}{\lambda_A}\left(\frac{g}{N}\right)^2\left(\frac{\hat{T}}{\bar{T}}\right)^2 \tag{1}$$

where g is the gravitational acceleration, $\hat{T}$ is the wave temperature amplitude, and $\bar{T}$ and $\bar{\rho}$ are the background temperature and density, respectively. These methods are inherently two dimensional, and the apparent horizontal wavelength λ_A is generally an overestimate of the true horizontal wavelength (Fig. 1a). Since the horizontal wavelength is in the denominator of (1), the momentum flux is therefore also generally under-estimated to the same degree. Examples of M_{2D} for January and July 2007 using the method described in Alexander et al. [2008] are shown in Figure S1.

2.3. COSMIC temperature profiles and three-dimensional gravity wave analysis

The COSMIC mission launched six low-earth-orbiting satellites with radio-occultation (RO) receivers in 2006. After a planned period of dispersal of the satellite orbits, the COSMIC mission provided nearly 2000 RO temperature profiles daily. We use focus here on measurements in 2007 when both COSMIC and HIRDLS were operational and coverage was near optimal for a full calendar year. RO gravity wave temperature anomalies are derived after removal of a background temperature using the same procedure as for HIRDLS (see S1).

The method we use here follows *Evan and Alexander* [2008] (see their Fig. 10) for a triad of profiles to determine horizontal wavenumber. The triad of profiles are assumed to be measured at the same time, and changes in phase between adjacent profiles are assumed due to the horizontal wavelength variations. We consider one RO profile and two HIRDLS profiles forming each triad. The nearest HIRDLS profile to the RO profile lies at the center of the coordinate system, which is illustrated in Figure 1b as the green circle. The red circle is the neighboring RO profile, and the blue circle is the second neighboring HIRDLS profile. λ_1 is the apparent wavelength determined along the blue line joining the two HIRDLS profiles, and λ_2 is the apparent wavelength along the red line joining the closest HIRDLS and RO profiles. The true propagation direction is illustrated in black with angle δ from east determined as:

$$\delta = \tan^{-1}\left(\frac{\lambda_2 \cos\theta_2 - \lambda_1 \cos\theta_1}{\lambda_1 \sin\theta_1 - \lambda_2 \sin\theta_2}\right), \tag{2}$$

where θ_1 is the angle of the blue line from east, and θ_2 is the angle of the red line from east. This formula discriminates between northwest-to-southeast and northeast-to-southwest wavenumber orientations, but give direction only with 180° ambiguity.

The analysis of horizontal phase difference between adjacent profiles to estimate horizontal wavenumber requires choosing a maximum time difference Δt and maximum horizontal spacing ΔR. The number of close coincidences found will be very sensitive to these choices, and smaller values decrease the number of profiles available for analysis considerably. For choosing Δt, consider typical frequencies resolved in limb-sounding data like

HIRDLS using the analysis of Preusse et al. [2008] and the sensitivity of limb-sounding measurement methods as a function of intrinsic frequency (see Alexander et al. [2010], their Figure 8). These methods are primarily sensitive to waves with intrinsic periods of approximate 2 hours and longer, suggesting a $\Delta t << 1$hr is desirable. With spacing between adjacent HIRDLS profiles ~100 km, and LOS averaging lengths $\sim 100 - -150$ km, we choose $\Delta R > 200$ km. For example, on day 151 out of a total of 5553 HIRDLS profiles and 1550 RO profiles available for this day, choosing Δt=20 min and ΔR=400 km results in only 101 RO profile close coincidences.

For each closely coincident RO profile found, we can form two triads of profiles and determine two values of horizontal wavelength and momentum flux. The HIRDLS profile measured prior to the closest coincidence forms the third member of one triad, and the HIRDLS profile measured after the closest coincidence forms the third member of the second triad.

For each triad, we perform the traditional 2D determination of horizontal wavelength to compute λ_1, then compute λ_2 for the same wave. We then solve (2) to get the true propagation direction δ, and compute wavelength λ_T from simple geometry. The true momentum flux is computed with (1), but substituting λ_A with λ_T to give true momentum flux, which we call the 3D flux. Here results are averaged over the height range of 17-22km to reduce random errors in the determination, and to give estimates of momentum flux in the lower stratosphere.

3. Results

3.1. Sensitivity to ΔR and Δt

As described in the previous section, the choice of Δt and ΔR has serious consequences for the amount of data remaining for the analysis. Several values were tested for Δt =10–20 min and ΔR =200–600 km. The number of profiles available for analysis is particularly sensitive to Δt in this range. Figure 2 shows the annual-mean and zonal-mean momentum fluxes for experiments using these ranges of values.

Mean horizontal wavenumber continues to shrink and momentum flux continues to increase with decreasing ΔR with no evidence of the results reaching a limit at the smallest value of ΔR=200 km. (See supporting information Figure S2.) Instead it appears clear that the spatial coverage of the data and associated profile spacing is still significantly limiting the retrieved gravity wave parameters. Sensitivity to Δt is relatively weak over this range, suggesting that most of the waves, at the wavelengths measured here, have ground based periods longer than a few hours. The data coverage is sparse at the smaller limits, so for the remainder of the paper we will show results for ΔR=300 km and Δt=20 min. Figure 2 suggests that results for different choices will vary by only ±20%, but also suggests that with better sampling from future measurements, the fluxes derived might still significantly increase.

Focusing now on the results obtained with Δt=20min/ΔR=300km, we show distributions of the frequency of occurrence of different horizontal wavelengths and momentum fluxes in Figure 3, and compares the 2D and 3D methods. The median value of horizontal wavelength in the 2D and 3D methods is very similar, 270km and 250km respectively. However the mean value of the horizontal wavelength is much smaller using the

3D method. By resolving the propagation direction, many of the very long apparent horizontal wavelengths sampled with the 2D method are shorter when the third dimension is resolved. Rather than changing the peak in the horizontal wavelength distribution (the median), it is the shape of the distribution that is most affected. The distribution of momentum fluxes is similarly affected by resolving the 3D structure, where the tail of the distribution is most affected. These distributions show extended tails resembling those displayed over topography where intermittent large-amplitude waves occur in long-duration balloon measurements [*Herzog et al.*, 2012].

The mean momentum flux using the 2D method is 1.7 mPa, whereas with the 3D method it is 6.4 mPa, an increase by a factor of 3.7. The increase in mean horizontal wavenumber is a factor of 2.5, and this is the main reason for the increase in momentum flux via (1). (Mean wavenumbers increase from 1/888km using the 2D method to 1/354km using the 3D method). The additional 50% increase in the mean momentum flux is due to an increase in wave amplitudes that is afforded by including the sometimes favorable viewing angles of the RO line-of-sight (LOS), which generally lies at an angle to the HIRDLS LOS. Both measurements have similar LOS averaging lengths of ∼100–150 km, and the smaller horizontal wavelength waves are more sensitive to this viewing angle effect on amplitude. To take advantage of this viewing angle effect in our calculations, we use the larger value of covariance $\hat{T}^2$ between the two arms of the triad in Fig. 1b rather than the average value.

3.2. Latitudinal and Seasonal Variations

3.2.1. Momentum flux

With Δt=20 min and ΔR=300 km, we have sufficient global coverage to examine latitudinal and seasonal variations in momentum flux. Figure 4 shows results. While the global mean momentum flux is 3.7 times larger with the 3D method, the increase is not globally uniform. Increases are largest near the equator and in the Northern Hemisphere midlatitudes.

Figure 4 also shows the 3D method zonal and meridional momentum fluxes separately. Fluxes are primarily zonal near the equator and Northern Hemisphere midlatitudes, and these are the latitudes where the HIRDLS measurement track is aligned more meridionally. At the higher latitudes sampled in the Northern and Southern Hemispheres, the fluxes are more equally divided between zonal and meridional. These are latitudes where the sampling is transitioning to purely zonal at the turnaround latitudes of the measurement track. Figure 5 illustrates the HIRDLS sampling and preferential projection of the 2D method onto waves propagating at different angles. This sampling effect convolved with the preferential wave propagation directions at different latitudes explains the latitudinal variations in increased flux seen with the 3D method.

4. Discussion & Conclusions

The focus in this work is on gravity wave momentum fluxes in the lower stratosphere at levels between 17 and 22 km, above clouds that block HIRDLS infrared measurements, but low enough to provide information on how the waves will affect the circulation above.

Including COSMIC RO profiles limits the maximum height that can be studied to 40km. This reduces the maximum vertical wavelengths we can examine to ~20 km, which may decrease the zonal mean momentum fluxes, particularly in SH winter, where mountain waves and other westward propagating waves grow to very long vertical wavelengths and the highest momentum fluxes are seen.

Decreasing the maximum time difference allowed between neighboring profiles (Δt) reduced the amount of data approximately proportionally. Changes in Δt for values less than 20 min had only minor effects on the average derived gravity wave parameters, confirming previous work that suggested waves observed by limb-sounding were primarily sensing waves with periods of 2 hrs and longer. Decreasing the allowed distance between neighbors (ΔR) also reduces the amount of data proportionally, however changes in ΔR had a large effect on the retrieved gravity wave parameters, a result also noted by *Faber et al.* [2013] over a range of longer ΔR. Smaller ΔR results in smaller retrieved horizontal wavelengths, but the decrease is less than proportional. Decreasing ΔR by a factor of three (from 600 to 200 km) resulted in continued decreases in retrieved horizontal wavelength and increases in momentum flux. These changes do not appear to saturate at ΔR=200 km, but instead indicate that better sampling would continue to change the results. Latitudinal and seasonal variations are however insensitive to these limits.

The 3D retrieval gives true horizontal wavenumbers that are roughly a factor of 2 larger than the apparent wavenumbers derived from the 2D method. This increase in wavenumber (decrease in wavelength) varies from a factor of 1.6 to 2.1 depending on the value of ΔR.

Momentum flux scales as the inverse of horizontal wavelength, but the 3D method gives momentum fluxes that are 3.3 to 5.6 times larger, depending on the value of ΔR chosen. These factors are larger than expected from changes in horizontal wavelength alone. The additional increases come from increases in wave temperature amplitudes that result from including RO profiles. The LOS angle relative to lines of constant phase can affect the observed wave amplitude for wavelengths shorter than several hundred km. The addition of the RO profiles to HIRDLS adds randomly oriented LOS angles that sometimes give more favorable observing geometry. RO will also observe larger amplitudes for the shortest vertical wavelength gravity waves due to slightly better vertical resolution [*Wright et al.*, 2011]. In the average, this gives an additional increase in wave amplitude of 45-60%, and since momentum flux increases with the square of wave amplitude, this gives an additional increase in momentum flux by a factor of 2.1-2.6.

We did not test ΔR smaller than 200 km because sampling becomes so poor that global patterns are increasingly dominated by poor statistics. It is questionable whether there is real value in choosing $\Delta R < 200$ km because there are limits on the resolution of gravity waves associated with the LOS integration path inherent in limb-sounding measurements. This integration length is $\sim$150 km, so on average, horizontal wavelengths observed with limb-sounding methods are not expected to be much shorter than 200 km. Indeed, our results show that the median horizontal wavelength is almost unchanged between the 2D and 3D methods. Hence, the results for ΔR=200 km may be showing something close to the limits of the method. Those results, although too noisy to reveal clear global patterns, can give global-mean corrections that may be representative of the "best estimate" of true correction factors that would be obtained with optimal sampling. These correction factors are on average approximately a factor of two decrease in horizontal wavelength and a factor of five increase in momentum flux, but with significant variations with latitude.

Considering again the comparison in *Geller et al.* [2013] between HIRDLS 2D momentum fluxes and parameterized gravity wave momentum fluxes in climate models suggests the new 3D fluxes are comparable or larger than the models. Larger fluxes may be warranted since the models are tuned primarily to reproduce mesospheric winds and temperatures, while additional flux from large-amplitude waves may drive circulation preferentially at stratospheric levels where model biases remain a common problem.

Future measurements from COSMIC-2 have great promise for providing a larger number of profile coincidences, however because both space and time restrictions must be applied, even these high-density measurements will likely still undersample the globe. However the improvements in sampling should be great enough that with sustained measurements over many years, robust global patterns in gravity wave parameters may be obtained.

The results here show interesting variations in wave propagation direction. A majority of waves at latitudes from 40°S to 70°N propagate zonally. Our estimates are that 70-85% of the momentum flux is zonal at these latitudes. At mid-to-high southern latitudes, this pattern changes to where there is less preference for either zonal or meridional propagation. We interpret this as the tendency for waves to propagate southwest or northwest on either side of the stratospheric vortex wind maximum in fall-winter-spring, and that large momentum fluxes in this season dominate the mean. The pattern is seen in observations and models [*Preusse et al.*, 2002; *Alexander and Teitelbaum*, 2007, 2011; *Sato et al.*, 2012] and likely related to horizontal refraction of wave propagation directions associated with strong wind gradients in the Southern Hemisphere stratospheric jet [*Sato et al.*, 2009, 2012].

These results suggest large corrections to previous interpretations of gravity wave drag inferred from limb sounding observations. *Ern et al.* [2011] showed "potential accelerations" associated with vertical gradients in momentum fluxes and referred to these gradients as "gravity wave drag" in a second paper focusing on tropical latitudes [*Ern et al.*, 2014]. Our results suggest potentially large errors associated with interpreting these gradients as "drag". First, the momentum fluxes estimated with the two-dimensional methods are likely too small by a factor of five, a factor that would proportionately affect the inferred gradient in the drag. Second, the fraction of waves propagating zonally and meridionally changes with latitude, and hence gradients in fluxes cannot easily be interpreted as zonal drag forces. Finally, there can be gradients in momentum fluxes associated solely with observational limitations even without any wave dissipation and drag. For example, if vertical wavelengths grow longer or shorter than the observable range, then the flux can decrease without any true drag acting on the circulation. Rather than providing constraints on drag, these global observations are best used to constrain momentum flux.

Acknowledgments. This work was supported by the NASA Aura Science Team–Atmospheric Composition Program through grant #NNX14AE82G. COSMIC RO temperature profiles are freely available from the UCAR CDAC website at http://cdaac-www.cosmic.ucar.edu/cdaac/products.html. HIRDLS temperature profiles are available through the NASA Goddard Earth Sciences Data Information Services Center at http://disc.sci.gsfc.nasa.gov/Aura/data-holdings/HIRDLS/index.shtml.

References

Alexander, M. J., and H. Teitelbaum (2007), Observation and analysis of a large amplitude mountain wave event over the Antarctic Peninsula, *J. Geophys. Res.*, *112*(D21103), doi:10.1029/2006JD008,368.

Alexander, M. J., and H. Teitelbaum (2011), Three-dimensional properties of Andes mountain waves observed by satellite: A case study, *J. Geophys. Res.*, *116*(D23110), doi:10.1029/2011JD016,151.

Alexander, M. J., J. Gille, C. Cavanaugh, M. Coffey, C. Craig, V. Dean, T. Eden, G. Francis, C. Halvorson, J. Hannigan, R. Khosravi, D. Kinnison, H. Lee, S. Massie, and B. Nardi (2008), Global estimates of gravity wave momentum flux from High Resolution Dynamics Limb Sounder (HIRDLS) observations, *J. Geophys. Res.*, *113*(D15S18), doi:10.1029/2007JD008,807.

Alexander, M. J., M. Geller, C. McLandress, S. Polavarapu, P. Preusse, F. Sassi, K. Sato, S. D. Eckermann, M. Ern, A. Hertzog, Y. Kawatani, M. Pulido, T. Shaw, M. Sigmond, R. Vincent, and S. Watanabe (2010), Recent developments in gravity wave effects in climate models, and the global distribution of gravity wave momentum flux from observations and models, *Q. J. Roy. Meteorl. Soc.*, *136*(DOI:10.1002/qj.637), 1103–1124.

Anthes, R. A., P. A. Bernhardt, Y. Chen, O. Cucurull, K. F. Dymond, D. Ector, S. B. Healy, S.-P. Ho, D. C. Hunt, Y.-H. Kuo, H. Liu, K. Manning, C. McCormick, T. K. Meehan, W. J. Randel, C. Rocken, W. W. Schreiner, S. V. Sokolovskiy, S. Syndergaard, D. C. Thompson, K. E. Trenberth, T.-K. Wee, N. L. Yen, and Z. Zeng (2008), The COSMIC/FORMOSAT-3 Mission, early results, *Bull. Am. Meteorol. Soc.*, *89*, 313–333.

Butchart, N., A. J. Charlton-Perez, I. Cionni, S. C. Hardiman, P. H. Haynes, K. Krueger, P. J. Kushner, P. A. Newman, S. M. Osprey, J. Perlwitz, M. Sigmond, L. Wang, H. Akiyoshi, J. Austin, S. Bekki, A. Baumgaertner, P. Braesicke, C. Bruehl, M. Chipperfield, M. Dameris, S. Dhomse, V. Eyring, R. Garcia, H. Garny, P. Joeckel, J.-F. Lamarque, M. Marchand, M. Michou, O. Morgenstern, T. Nakamura, S. Pawson, D. Plummer, J. Pyle, E. Rozanov, J. Scinocca, T. G. Shepherd, K. Shibata, D. Smale, H. Teyssedre, W. Tian, D. Waugh, and Y. Yamashita (2011), Multimodel climate and variability of the stratosphere, *J. Geophys. Res.*, *116*(D05102), doi:10.1029/2010JD014,995.

Ern, M., P. Preusse, J. C. Gille, C. L. Hepplewhite, M. G. Mlynczak, J. M. Russell III, and M. Riese (2011), Implications for atmospheric dynamics derived from global observations of gravity wave momentum flux in stratosphere and mesosphere, *J. Geophys. Res.*, *116*(D19107), doi:10.1029/2011JD015,821.

Ern, M., F. Ploeger, P. Preusse, J. C. Gille, L. J. Gray, S. Kalisch, M. G. Mlynczak, J. M. Russell, and M. Riese (2014), Interaction of gravity waves with the QBO: A satellite perspective, *Journal of Geophysical Research: Atmospheres*, *119*(5), 2329–2355, doi: 10.1002/2013JD020731.

Evan, S., and M. J. Alexander (2008), Intermediate-scale tropical inertia gravity waves observed during TWP-ICE campaign, *J. Geophys. Res.*, **113**, doi:10.1029/2007JD009,289.

Faber, A., P. Llamedo, T. Schmidt, A. de la Torre, and J. Wickert (2013), On the determination of gravity wave momentum flux from GPS radio occultation data, *Atmospheric Measurement Techniques*, *6*(11), 3169–3180, doi:10.5194/amt-6-3169-2013.

France, J. A., V. L. Harvey, M. J. Alexander, C. E. Randall, and J. C. Gille (2012), High Resolution Dynamics Limb Sounder observations of the gravity wave-driven elevated stratopause in 2006, *Journal of Geophysical Research: Atmospheres*, *117*(D20), 10.1029/2012JD017,958.

Geller, M. A., M. J. Alexander, P. E. Love, J. Bacmeister, M. Ern, A. Hertzog, E. Manzini, P. Preusse, K. Sato, A. A. Scaife, and T. Zhou (2013), A comparison between gravity wave momentum fluxes in observations and climate models, *J. Climate*, *26*, 6383–6405.

Gille, J. C., and et al. (2008), The High Resolution Dynamics Limb Sounder (HIRDLS): Experiment overview, recovery and validation of initial temperature data, *J. Geophys. Res.*, *113*(D16S43), doi:10.1029/2007JD008,824.

Herzog, A., M. J. Alexander, and R. Plougonven (2012), On the intermittency of gravity-wave momentum flux in the stratosphere, *J. Atmos. Sci*, *69*, 3433–3448.

Preusse, P., A. Dörnbrack, S. D. Eckermann, M. Riese, B. Schaeler, J. T. Bacmeister, D. Broutman, and K. U. Grossmann (2002), Space based measurements of stratospheric mountain waves by CRISTA 1. sensitivity, analysis method and a case study, *J. Geophys. Res.*, *107(D23)*(8178), doi:10.1029/2001JD000,699.

Sato, K., S. Watanabe, Y. Kawatani, Y. Tomikawa, K. Miyazaki, and M. Takahashi (2009), On the origins of gravity waves in the mesosphere, *Geophys. Res. Lett.*, *36*(L19801), doi:10.1029/2009GL039,908.

Sato, K., S. Tateno, S. Watanabe, and Y. Kawatani (2012), Gravity wave characteristics in the Southern Hemisphere revealed by a high-resolution middle-atmosphere general circulation model, *J. Atmos. Sci.*, *69*(doi: http://dx.doi.org/10.1175/JAS-D-11-0101.1), 1378–1396.

Schirber, S., E. Manzini, T. Krismer, and M. Giorgetta (2015), The quasi-biennial oscillation in a warmer climate: Sensitivity to different gravity wave parameterizations, *Climate Dynamics*, *45*(3-4), 825–836, doi:10.1007/s00382-014-2314-2.

Stockwell, R.G., L. Mansinha, and R. Lowe, R. (1996), Localisation of the complex spectrum: The S-Transform, *IEEE Trans. Sig. Proc.*, *44*(4), 998-1001.

Wang, L., and M. J. Alexander (2010), Gobal estimates of gravity wave parameters from GPS radio occultation temperature data, *J. Geophys. Res.*, *115*(D21), doi:10.1029/2010JD013860.

Wright, C. J., S. M. Osprey, J. J. Barnett, L. J. Gray, and J. C. Gille (2010), High Resolution Dynamics Limb Sounder measurements of gravity wave activity in the 2006 arctic stratosphere, *J. Geophys. Res.*, *115*(D02105), doi:10.1029/2009JD011,858.

Wright, C. J., M. B. Rivas, and J. C. Gille (2011), Intercomparisons of HIRDLS, COSMIC and SABER for the detection of stratospheric gravity waves, *Atmos. Meas. Tech.*, *4*, 1581–1591.

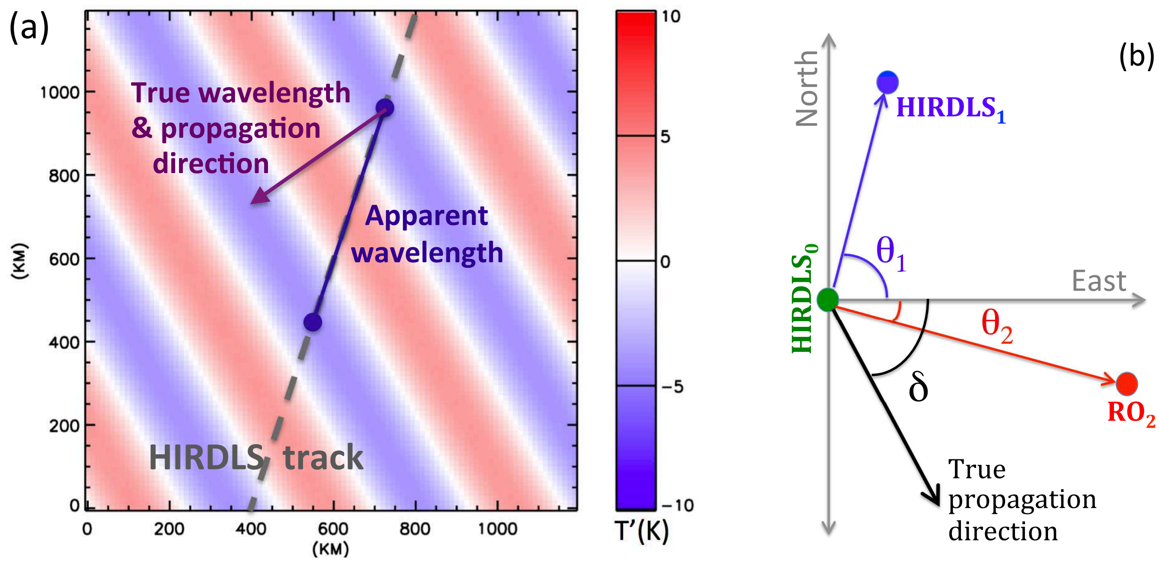

Figure 1. (a) Schematic depicting the apparent horizontal wavelength determined with HIRDLS data only versus the true horizontal wavelength. These are referred to as "2D" and "3D" methods, respectively. (b) Geometry for the 3D method described in section 2.

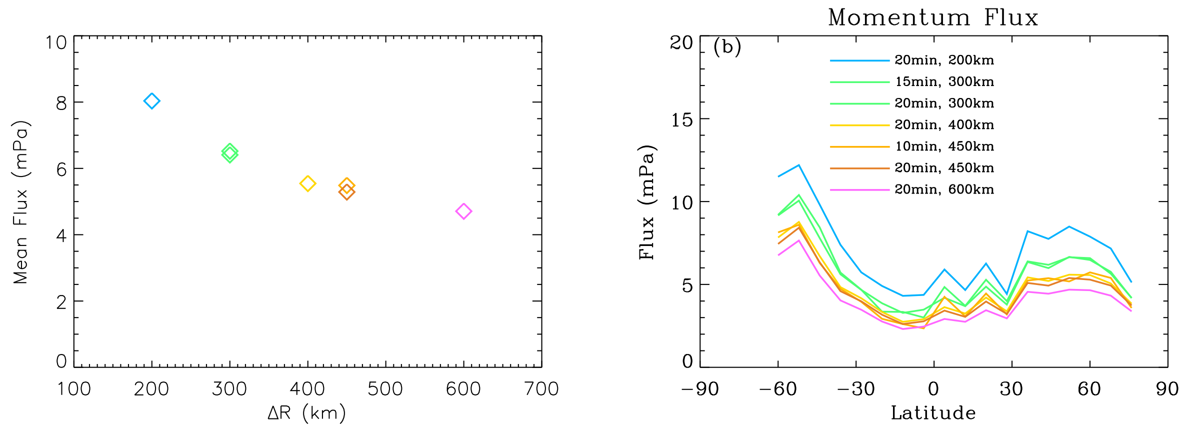

Figure 2. Left: Globally and annually averaged momentum flux as a function of ΔR. Color key is shown in the right panel. Similar colors have the same ΔR. Minor variations in color are associated with different Δt for the same ΔR. Sensitivity of the flux to Δt is weak compared to ΔR. Right: Momentum flux versus latitude showing sensitivity of annual-mean, zonal-mean gravity wave momentum flux to ΔR and Δt.

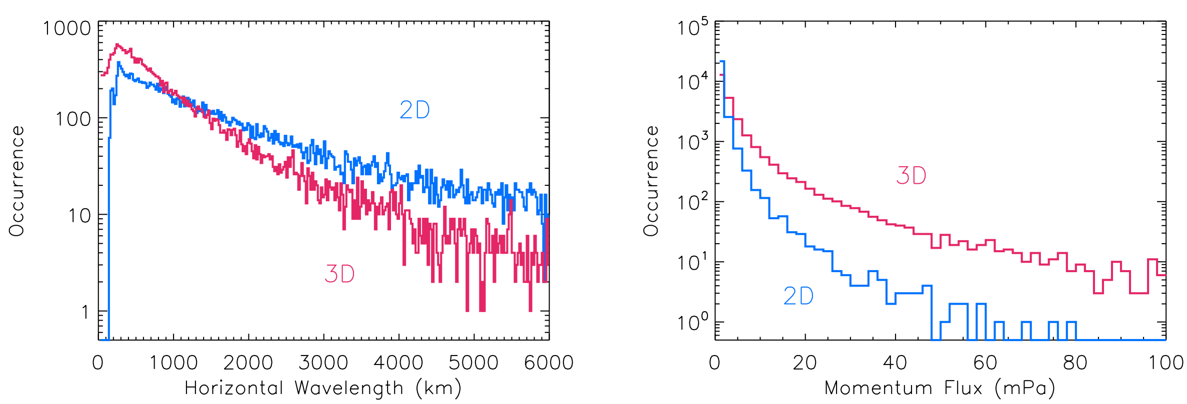

Figure 3. Left: Frequency of occurrence of horizontal wavelength using the 2D (blue) and 3D (red) methods. Right: Frequency of occurrence of momentum flux using the 2D (blue) and 3D (red) methods.

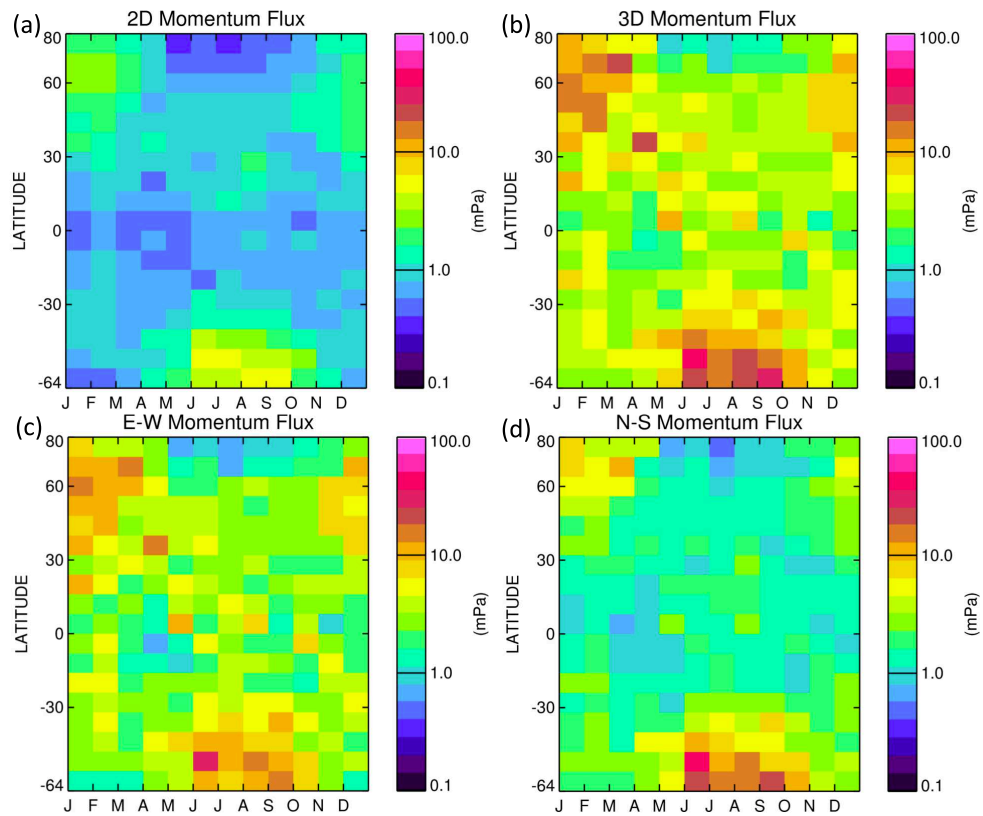

Figure 4. Absolute value of momentum flux versus month of the year 2007 and latitude. (a) Total flux with the 2D method. (b) Total flux with the 3D method. (c) Zonal flux with the 3D method. (d) Meridional flux with the 3D method.

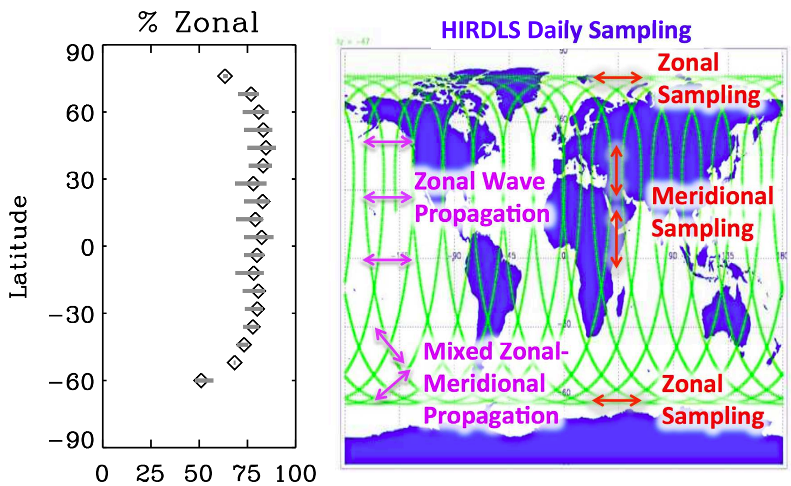

Figure 5. Left: Percent of waves with zonal propagation versus latitude. The gray bars show the range of values computed for different ΔR. Right: Schematic map showing daily HIRDLS measurement tracks (green). The red arrows and notation show the tendency for meridional sampling to occur near the equator and at Northern Hemisphere midlatitudes, transitioning to zonal sampling at the turnaround latitudes (64°S and 80°N). Purple arrows and notiation show the preferential wave propagation directions found in this study.